The 4th Canadian Conference on Nonlinear Solid Mechanics (CanCNSM 2013)
McGill University, July 23-26, 2013
Montreal, Canada

Paper ID 655

Failure mechanisms in rapid-prototyped polymer microtrusses

Abstract
Optimally designed microtrusses typically contain a complex internal geometry that can be difficult to fabricate from high-strength materials. One way of synthesizing this type of architecture is through a combination of rapid prototyping and electrodeposition wherein the polymer core acts as a template for a high-strength nanometal. Net-shape manufacturing methodology can give enhanced freedom to architectural selection allowing microtrusses to be designed for applications like vibration dampeners, heat exchangers, and ultra-lightweight sandwich panels. This study analyzes the as-printed polymer microtrusses tested in three-point bending to extract mechanical properties, while three-dimensional digital image correlation and scanning electron microscopy were used to characterize the relevant failure mechanisms.

Keywords
failure mechanisms – buckling – rapid prototyping – microtruss – digital image correlation

Ante LAUSIC, Department of Materials Science and Engineering, University of Toronto, ante.lausic@utoronto.ca
Craig STEEVES, University of Toronto Institute of Aerospace Studies, csteeves@utias.utoronto.ca
Glenn HIBBARD, Department of Materials Science and Engineering, University of Toronto, glenn.hibbard@utoronto.ca

Introduction

Cellular materials as a class contain common structures such as foams, honeycombs and hybrids thereof. Microtrusses, however, are more efficient than foams and comparable to in-plane honeycombs for weight specific applications [1-3] and as such have garnered interest in aerospace and automotive industries for application ranging from heat exchangers to energy absorbers [4-6]. They consist of struts connected in various geometries (tetrahedral, octahedral, etc.) that can be combined with solid or porous face sheets to synthesize composite sandwich panels. This structure allows applied loads to be transmitted axially along the core struts such that they act as stretch dominated structures in contrast to the bending dominated architectures in foams.

Microtrusses can be manufactured in multiple ways from bulk material (see work on deformation forming [7], weaving [8], stacking [9], and investment casting [10]) but it is difficult to directly make them from high-strength materials due to various manufacturing limitations. While casting, for example, has great flexibility in the freedom of shape and can create complex architectures, small internal cross-sectional dimensions can lead to internal flaws that weaken the final structure [11].

An alternative method was developed wherein a polymer template was fabricated via 3D printing, a type of rapid prototyping, followed by nanocrystalline Ni electrodeposition [12]. This method has the same flexibility to produce complex architectures as casting with current manufacturing technology having resolution down to 10µm. Subsequently, the coating process has the ability to encapsulate the polymer core with a high strength nanocrystalline metal. This creates a metal/polymer microtruss hybrid with significant freedom in architecture and material choice. Technical challenges for this approach include metallization of the polymer and polymer surface roughness.

This study examines the structure of the pre-coated rapid prototyped polymer microtrusses with a combination of three-point bending, digital image correlation (DIC) and scanning electron microscopy (SEM). Samples were tested in three-point bending to simulate applications where truss-like structures have been shown to be the topologically optimal structure for supporting a central load (e.g. [3]).

1. Methodology

Microtruss beams were fabricated in a 3D Systems ProJet 3500 HD rapid prototyper using Visijet Crystal polymer part material [13]. Because of the need for wax supports in

complex structures during printing, samples were placed in a 3D Systems Finisher at 65°C to melt away these supports. Next, samples were rinsed in a heated ultrasonic bath to remove residual wax and then washed with soapy water. Specimens were also set aside for speckle coating in the DIC measurements.

Three-point bending tests were performed in a 50kN Shimadzu universal testing machine at a cross-head displacement of 1mm/min. DIC measurements were performed using a pair of GOM 5M cameras synchronized to an ARAMIS DIC system [14]. Electron micrographs were taken with a Hitachi SU3500 SEM.

2. Polymer microtrusses

Microtrusses composed of square pyramidal unit cells were rapid-prototyped with circular struts 6.25mm long and 0.625mm in radius corresponding to a slenderness ratio of 20. The core struts connecting the face sheets were inclined at 45 degrees and the finished beam was 3 unit cells wide and 11 unit cells long. Four specimens were tested and showed good repeatability with an average peak force of 54.8±0.2N and peak deflection of 6.0±0.1mm before fracture (Fig. 1).

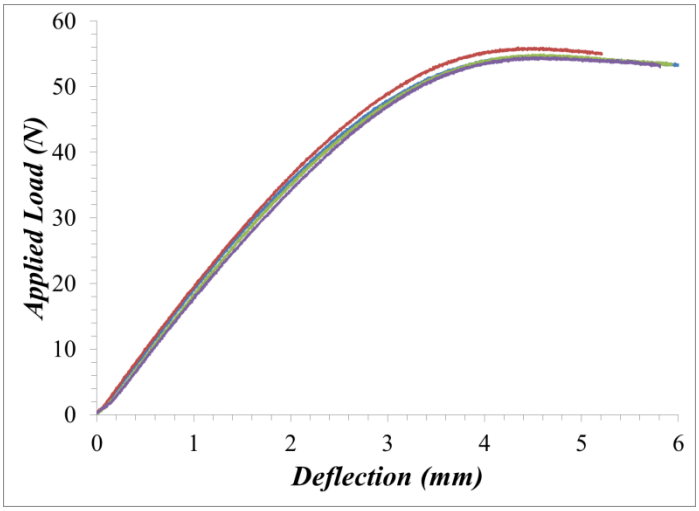

Figure 1: Force-deflection curves for polymer microtrusses where struts had a slenderness ratio of 20 both in the face and in the core.

2.1 Fracture mechanism in polymer microtrusses

Upon failure, the microtruss beam broke into two pieces down the center (Fig. 2a) but the exact location of failure initiation was difficult to interpret. If the truss is reassembled, all the struts in the fracture zone can be accounted for except for one outer face sheet strut on the bottom of the microtruss (Fig. 2b). This failure mode was common among all four tested specimens in this set.

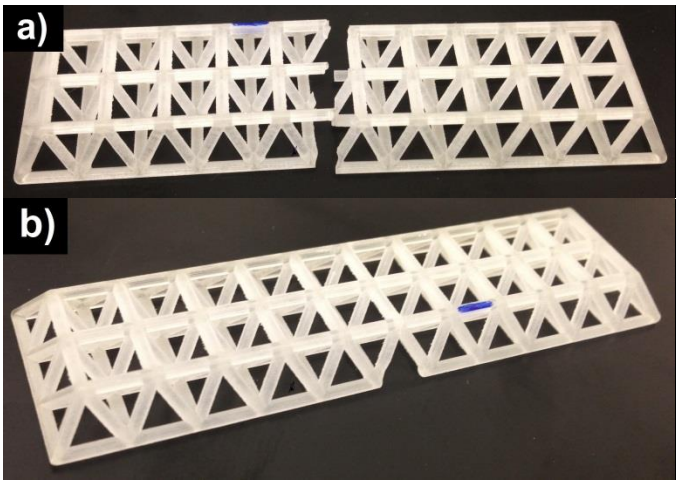

Figure 2: Microtruss beam with slenderness ratio of 20 (a) after failure and (b) reassembled with the notable absence of a central face strut at the outside edge.

DIC measurements show a spatially varying strain across the truss and within each strut (Fig. 3b). The highest concentrations of strain are found to be along the bottom face sheet struts directly beneath the central roller. At the center of 'Strut 1' (Fig. 3b), the maximum measured strain was 3.8% while at either end of the same strut, the maximum value was higher at 4.3%. The adjacent strut (labelled 'Strut 2') had a lower strain of 2.4% and the strains continuously decrease towards both ends of the beam, symmetrically. This trend is also seen in the top face sheet struts but not to the same degree. The highest recorded strain in the top face sheet was 4.0% directly below the central roller but fell off quickly to an average of 1.5% in 'Strut 3' directly adjacent to the center node.

Failure is then attributed to the face sheet struts on the bottom of the microtruss (those in tension) breaking away from the nodes on either side as is noted by the absence of this strut joining these high-strain nodes. The preference to breakage at the node and not mid-strut is related to the stress concentrations that exist at points of curvature where the strut meets other struts at a common node. DIC images at 3mm deflection (halfway to failure) show these higher strain values at the ends of the strut near the node.

Initial fracture in the outer face sheet strut requires a redistribution of the load in the system leading to an imbalance in the microtruss, parallel to its length. This creates a preference for the microtruss to bend towards the side that has already lost a strut. With this in-plane flexure, the core struts that lead to the top face are now bending away from each other and their connection at the node is undergoing fracture (Fig. 4a). Because the tensile stress is normal to the plane of the crack, it is considered Mode 1 fracture, an opening mode type of crack propagation where the surfaces are moving directly apart [15].

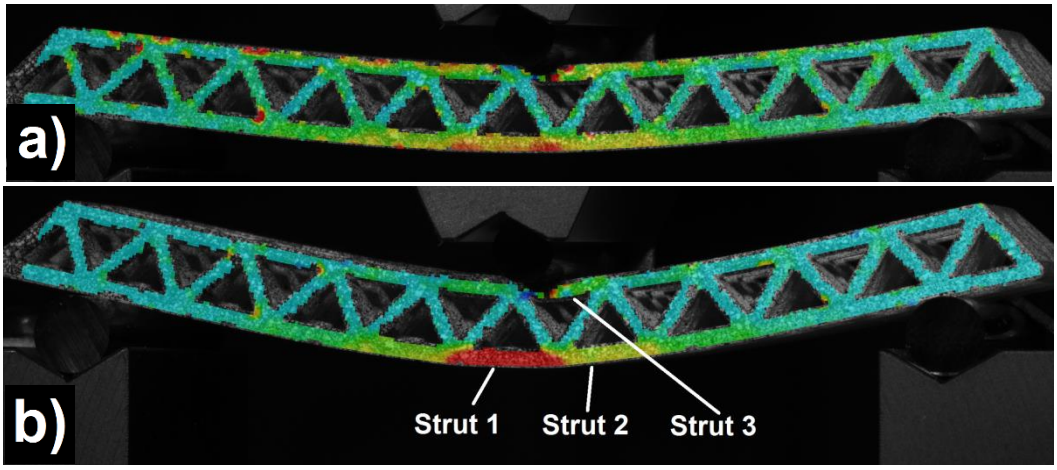

Figure 3: DIC major strain measurements showing the strain distribution (a) at 3mm deflection and (b) immediately before failure.

SEM was performed on the failed samples to examine the fracture surfaces of the sample in detail. The nodes that had core struts bending away in different directions resulted in fracture that not only went through the node but also partially through the core strut itself (Fig. 4b). These breaks are not oriented in the direction of printing and therefore are not due to the joining of subsequent layers in the printing process but instead suggest Mode I fracture.

Together with SEM micrographs, DIC measurements and reassembly of the microtruss after fracture, the mechanism is understood as a simultaneous fracture at both ends of the outer face sheet strut on the bottom of the microtruss beam.

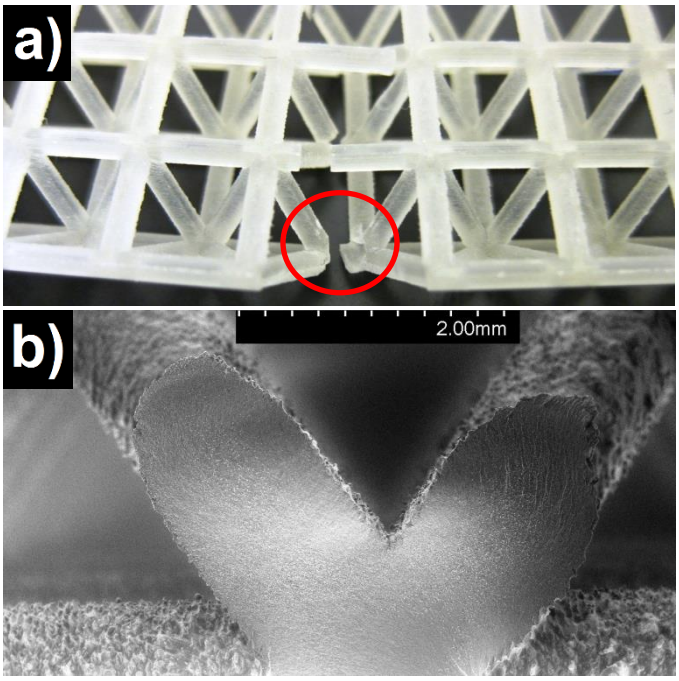

Figure 4: (a) View of the microtruss beam from underneath. The core struts separate after the bottom face strut has failed leading to fracture through the node (indicated by the red circle). (b) SE micrograph showing the fracture surface at the node which exhibits Mode I fracture.

2.2 Preference for fracture in bottom face sheet

While the DIC results do show the preference for the bottom face sheet struts to be more significantly deformed than the struts in the top face sheet, a rationale for why this is cannot be directly extracted from the images. Instead, the forces within each sheet and their struts can be derived to explain this.

Equation 1 converts the load being applied by the apparatus to a force in the struts in both face sheets [16], where P is the applied load, L is the length of the beam and d is the centroid to centroid distance between the face sheets. By then dividing by the area in a cross-sectional slice of the face sheet away from the nodes, the stress in those struts is obtained. For the top face sheets, only three struts hold all the force and thus have total area $3\pi r^2$ while the bottom face sheet has total area $4\pi r^2$. This means the stress in the top face sheet struts is 4/3 times higher than those in the bottom ones.

$$F = \frac{PL}{4d} \qquad (1)$$

With this result, it may be expected that the top sheet should break first. However, the polymer behaves differently in compression and in tension. The ultimate tensile strength (UTS) of this material based on ASTM D638 tests is 30.2MPa [17] while the 0.2% offset yield strength in compression according to ASTM D695 is 44MPa [18].

Assume the scenario at which the bottom face sheet strut fails at its 30.2MPa maximum. Multiplying by the 4/3 ratio gives the corresponding stress of 40MPa in the top face sheet. This value is still below the 44MPa yield strength of the polymer in compression and, thus, the bottom will break first.

3. Reduced core polymer microtrusses

In direct compression, the loads in the oblique core struts of microtrusses are large relative to the loads in the face struts [12] and govern failure of the structures. By contrast, in a microtruss beam in three-point bending, the oblique core struts are loaded relatively lightly compared to the face struts; see the difference in strains between the face struts and core struts shown in Fig. 3. In bending, the oblique core struts are not critical points of failure and their mass is partly parasitic. The total mass of the structure can therefore be reduced by decreasing the size of the core struts while leaving the face struts unchanged. The limits of this are tested experimentally in the following section.

3.1 Sample selection for reduced core microtrusses

Microtruss beams were created with face sheet struts having a radius of 0.625mm (identical to the baseline microtruss beam in section 2) and core struts having radii ranging from 0.5mm to 0.25mm. Table 1 provides the sample geometries and masses for each structure. All beams were of the same length and width (± one strut diameter) and the same total thickness. These thinner core struts had slenderness ratios ranging from 22 to 31 resulting in reductions of volume over the standard face sheet strut size (V_r) of 80 to 40%

Table 1: Geometries of reduced core polymer microtrusses

Name	Core Strut Radius (mm)	Slenderness Ratio	V_r (%)	Mass (g)
NG	0.62	20	100	2.02
G1	0.56	22	80	1.82
G2	0.52	24	70	1.77
G3	0.48	26	60	1.67
G4	0.44	28	50	1.57
G5	0.42	30	45	1.49
G6	0.40	32	40	1.44

3.2 Three-point bend tests on reduced core microtrusses

For small reductions in the radius of the core struts (specimens G1-G3) the maximum bending load is constant and equal to the maximum bending load for the baseline beam, approximately 55 N. The maximum bending load for all specimens is shown in Fig. 5. The failure event was similar to the baseline beam failure: sudden and catastrophic. It is believed that failure in all cases is attributable to the stresses in the tensile face exceeding a critical level, leading to brittle failure in a single strut that rapidly propagated through the width of the structure and fracturing the beam into two pieces (Fig. 6).

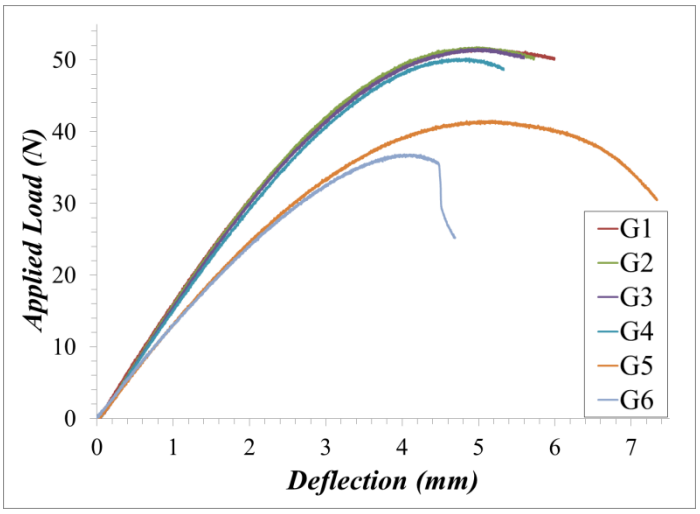

Figure 5: Force-deflection curves for the six reduced core microtruss beams from specimen G1 to G6 by volume thinner core struts. Specimens G1 thru G3 show almost no change.

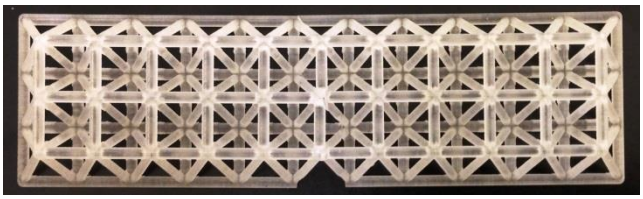

Figure 6: Reassembly of specimen G3 after three-point bend testing resulted in complete fracture of the beam.

With further reductions in the radii of the core struts (specimens G5-G6), the behaviour at failure of the microtruss beams changed markedly. Rather than catastrophic failure including fracture of the beam into two parts, failure was marked by buckling of the struts in the compressive face (see Fig. 7) and the peak measured load was lower than for the baseline beam. (Specimen G4 was intermediate between specimens G3 and G5.)

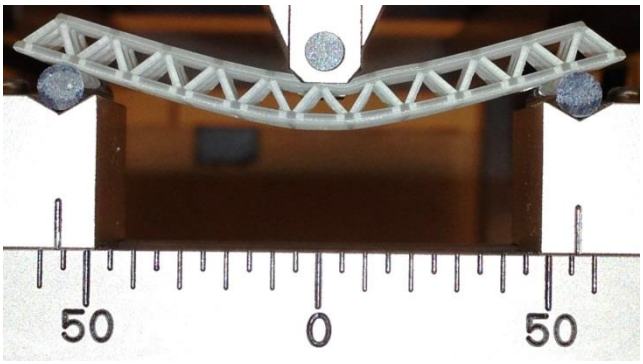

Figure 7: Three-point bend test for specimen G5 showing the buckling of the top face sheet strut directly to the right of the central roller.

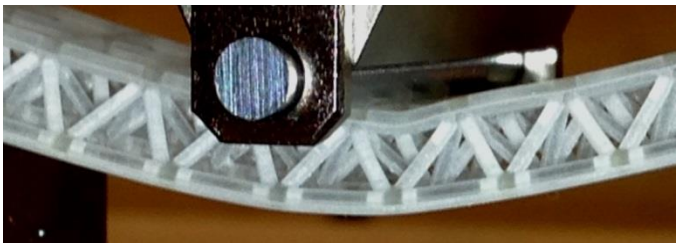

Figure 8: Close up view of specimen G5 at 5mm deflection from a side view showing a face sheet strut buckling to the right of the central roller.

When SEM imaging was to be done on the specimens, the truss was observed to have returned to its original state without any evidence of the face sheet buckling seen in the testing snapshots (Fig. 8). This relaxation and return to the original shape is evidence of the elastic nature of the polymer material.

In the electron microscope, bright white sections appeared on the struts due to charging on the surface of the specimen. Since a large depth of field was required for images on this small magnification, the secondary electron (SE) mode was utilized with the downside of higher accelerating voltage and vacuum leading to the charging (Fig. 9a). For higher magnification images, Ultra Variable-Pressure Detector (UVD) mode was utilized as depth of field was no longer essential. This removed the charging effect seen in SE mode and showed detail on the strut level such as some increase in cross-sectional area at the midpoint of the strut and bulging/deformation along the sides of the strut (Fig. 9b).

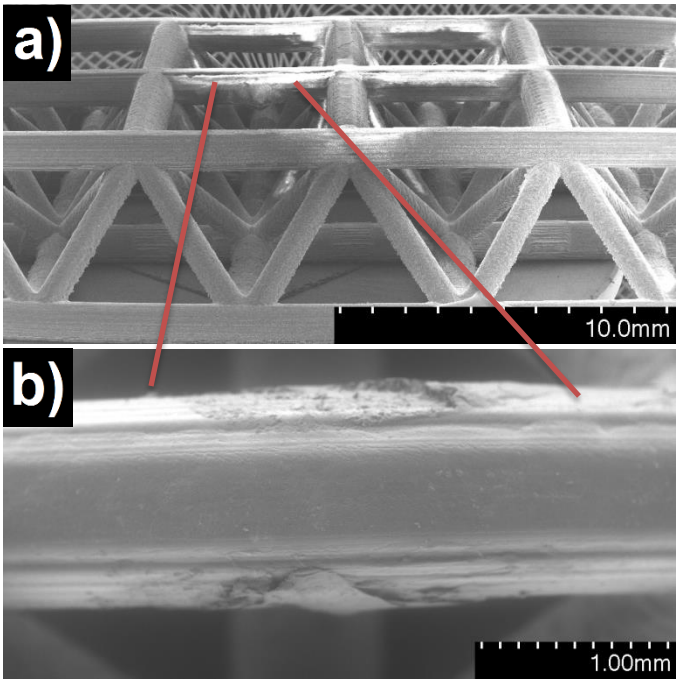

Figure 9: SE and UVD micrographs of specimen G5 after face sheet buckling failure. Relaxation of the polymer returns it to its starting shape (a) but evidence of buckling is still seen in the central face sheet strut at its midpoint (b).

3.3 Failure mechanism boundary

These results indicate that face failure of the microtruss sandwich beam in bending is subject to multiple competing mechanisms. It is believed that the reduction in the size of the core struts reduced the rotational constraint on the face struts, increasing their propensity to buckle. For robust core struts, the constraint that the core supplies against face strut buckling is large and the face struts fail by yielding or brittle fracture. As the core struts become more slender, this constraint is relaxed and eventually the face struts are subject to buckling failure. As the core strut radii are reduced further, the load carrying capacity of the beam is also reduced. In figure 10 these competing mechanisms are represented by zones of fracture and face sheet buckling (FSB); at a given core geometry, the mechanism capable of withstanding the least load is active. Eventually, as the core struts are further reduced in size, buckling of the core struts themselves becomes the active failure mechanism, although this is not shown in figure 5.

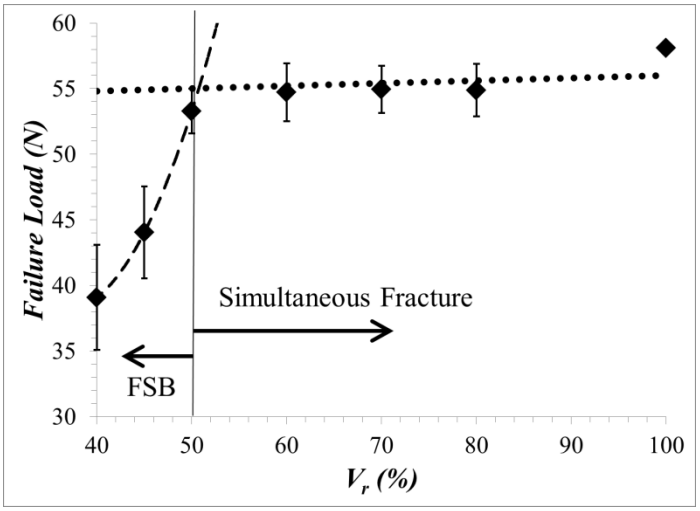

Figure 10: Nearly constant failure load as the core is thinned from 100% to 50% (fitted linearly by the dotted line). A shift in failure mechanism results in the dip after 50% as the specimens begin to face sheet buckle (FSB) (fitted quadratically by the dashed line).

The activation of buckling can be predicted using Euler's buckling formula (Equation 2), where E is the Young's modulus of the material, I is the second moment of area, L is the length of the beam and k represents the constraint conditions of the ends of the strut. It is likely the evolution of the effective end constraint (k) with decreasing core strut radius that governs the switch in failure mechanism from brittle fracture to buckling. The relationship between k and the core geometry is the subject of ongoing study.

$$F = \frac{k^2 \pi^2 EI}{L^2} \qquad (2)$$

Conclusion

Three-point bending tests of rapid-prototyped polymer microtruss beams showed a preference for fracture at face sheet nodes on the underside of the beam. Reassembling the broken microtruss showed simultaneous fracture at two points on the bottom that resulted in the expulsion of a complete strut. Coupled with DIC and SE micrographs, it is hypothesized that fracture propagation starts at one edge of the beam (in width) and works its way into the rest of the microtruss – all of which happens suddenly. DIC also showed the lack of strain in the core struts implying they are over-designed. By reducing their size compared to the face sheet strut size, a decrease in mass is possible while maintaining nearly the same load carrying capacity. Eventually the failure mechanism changes from simultaneous fracture at the nodes to buckling of the face struts adjacent to the force application point.

Acknowledgements

Financial support from the Natural Sciences and Engineering Research Council of Canada (NSERC) is gratefully acknowledged.

References

[1] – M. F. Ashby. Hybrids to fill holes in material property space. *Philo. Mag.*,85(26-27): 3235-3257, 2005.
[2] – V. S. Deshpande, M. F. Ashby and N. A. Fleck. Foam topology bending versus stretching dominated structures. *Acta Mater.*, 49: 1035-1040, 2001.
[3] – O. Sigmund. Topology optimization: a tool for the tailoring of structures and materials. *Phil. Trans. R. Soc. Lond. A.*,358: 211-227, 2000.
[4] – D. T. Queheillalt and H. N. G. Wadley. Cellular metal lattices with hollow trusses. *Acta Mater.*, 53: 303-313, 2005.
[5] – M. F. Ashby. The properties of foams and lattices. *Phil. Trans. R. Soc. A*, 364: 15-30, 2006.
[6] – H. N. G. Wadley. Multifunctional periodic cellular metals. *Phil. Trans. R. Soc. A*, 364: 31-68, 2006.
[7] – D. J. Sypeck and H. N. G. Wadley. Cellular metal truss core sandwich structures. *Adv. Eng. Mater.*, 4(10):759-764, 2002.
[8] – S. Hyun and S. Torquato . Optimal and Manufacturable Two-dimensional, Kagomé-like Cellular Solids. *J. Mater. Res.* 17: 137-144, 2002.
[9] – D. J. Sypeck and H. N. G. Wadley. Multifunctional microtruss laminates: textile synthesis and properties. *J. Mater. Res.* 16(3): 890-897, 2001.
[10] – V. S. Deshpande and N. A. Fleck. Collapse of truss core sandwich beams in 3-point bending. *Int. J. Solids Struct.*, 38: 6275- 6305, 2001.
[11] – S. Ho, C. Ravindran and G. D. Hibbard. Magnesium alloy micro-truss materials. *Script. Mater.*, 62(1): 21-24, 2010.
[12] – L. M. Gordon, B. A. Bouwhuis, M. Suralvo, J. L. McCrea, G. Palumbo and G. D. Hibbard. Micro-truss nanocrystalline Ni hybrids. *Acta Mater.*, 57(3): 932-939, 2009.
[13] – 3D Systems, Inc. ProJet® 3500 HD and HDPlus Professional 3D Printers. Accessed May 1, 2013. www.printin3d.com.
[14] – GOM mbh. ARAMIS Digital Image Correlation. Accessed May 1, 2013. www.gom.com.
[15] – R.W. Hertzberg. Deformation and fracture mechanics of engineering materials, 4th edition. Wiley, 1996.
[16] – C. A. Steeves and N. A. Fleck. Collapse mechanisms of sandwich beams with composite faces and a foam core, loaded in three-point bending. Part I: analytical models and minimum weight design. *Int. J. Mech. Sci.*, 46: 561-583, 2004.
[17] – ASTM Standard D638. Standard Test Method for Tensile Properties of Plastics. ASTM International, West Conshohocken, PA, 2010.
[18] – ASTM Standard D695. Standard Test Method for Compressive Properties of Rigid Plastics. ASTM International, West Conshohocken, PA, 2010.